ARTICLE

Injectable Graphene Oxide/Hydrogel-Based Angiogenic Gene Delivery System for Vasculogenesis and Cardiac Repair

Arghya Paul,[†,‡,§] Anwarul Hasan,[†,§,∞] Hamood Al Kindi,[∥] Akhilesh K. Gaharwar,[⊥] Vijayaraghava T. S. Rao,[#] Mehdi Nikkhah,[†,§,×] Su Ryon Shin,[†,‡,§] Dorothee Krafft,[†,§] Mehmet R. Dokmeci,[†,§] Dominique Shum-Tim,[∥] and Ali Khademhosseini[†,‡,§,∠,¶,*]

[†]Biomaterials Innovation Research Center, Division of Biomedical Engineering, Brigham and Women's Hospital, Harvard Medical School, 65 Landsdowne Street, Cambridge, Massachusetts 02139, United States, [‡]Wyss Institute for Biologically Inspired Engineering, Harvard University, Boston, Massachusetts 02115, United States, [§]Biomaterials Innovation Research Center, Harvard-MIT Division of Health Sciences and Technology, Massachusetts Institute of Technology, Cambridge, Massachusetts 02139, United States, [⊥]Texas A&M University, 5024 Emerging Technology Building, College Station, Texas 77843, United States, [∥]Divisions of Cardiac Surgery and Surgical Research, McGill University Health Centre, The Royal Victoria Hospital, Room S8-73b, 687 Pine Avenue, West Montreal, Quebec H3A 1A1, Canada, [#]Neuroimmunology Unit, Department of Neurology and Neurosurgery, Montreal Neurological Institute and Hospital, McGill University, Montreal, Quebec H3A 1A1, Canada, [∠]Department of Maxillofacial Biomedical Engineering and Institute of Oral Biology, School of Dentistry, Kyung Hee University, Seoul 130-701, Republic of Korea, and [¶]Department of Physics, King Abdulaziz University, Jeddah 21569, Saudi Arabia. [∞]Present address: Biomedical Engineering, and Department of Mechanical Engineering, American University of Beirut, Beirut, 1107 2020, Lebanon. [×]Present address: School of Biological and Health Systems Engineering, Arizona State University, Tempe, Arizona 85287, United States.

ABSTRACT The objective of this study was to develop an injectable and biocompatible hydrogel which can efficiently deliver a nanocomplex of graphene oxide (GO) and vascular endothelial growth factor-165 (VEGF) pro-angiogenic gene for myocardial therapy. For the study, an efficient nonviral gene delivery system using polyethylenimine (PEI) functionalized GO nanosheets (fGO) complexed with DNA_{VEGF} was formulated and incorporated in the low-modulus methacrylated gelatin (GelMA) hydrogel to promote controlled and localized gene therapy. It was hypothesized that the fGO_{VEGF}/GelMA nanocomposite hydrogels can efficiently transfect myocardial tissues and induce favorable therapeutic effects without invoking cytotoxic effects. To evaluate this hypothesis, a rat model with acute myocardial infarction was used, and the therapeutic hydrogels were injected intramyocardially in the peri-infarct regions. The secreted VEGF from *in vitro* transfected cardiomyocytes demonstrated profound mitotic activities on endothelial cells. A significant increase in myocardial capillary density at the injected peri-infarct region and reduction in scar area were noted in the infarcted hearts with fGO_{VEGF}/GelMA treatment compared to infarcted hearts treated with untreated sham, GelMA and DNA_{VEGF}/GelMA groups. Furthermore, the fGO_{VEGF}/GelMA group showed significantly higher ($p < 0.05$, $n = 7$) cardiac performance in echocardiography compared to other groups, 14 days postinjection. In addition, no significant differences were noticed between GO/GelMA and non-GO groups in the serum cytokine levels and quantitative PCR based inflammatory microRNA (miRNA) marker expressions at the injected sites. Collectively, the current findings suggest the feasibility of a combined hydrogel-based gene therapy system for ischemic heart diseases using nonviral hybrid complex of fGO and DNA.

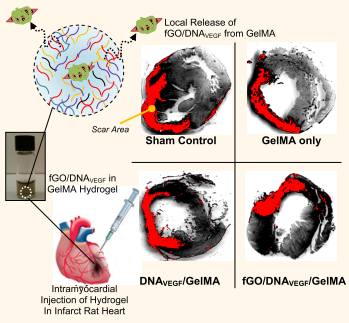

KEYWORDS: nanomedicine · graphene oxide · injectable hydrogel · gene delivery · myocardial therapy

Hydrogels have played an increasingly important role in tissue engineering.[1,2] This is mainly attributed to the unique properties of hydrogels including their high permeability, biodegradability, tunable physical properties, ability to provide structural support to bioengineered tissue constructs, as well as to surface coat medical implants for improved biocompatibility.[3,4] Hydrogels can also be made biofunctional by tethering suitable growth factors, therapeutic peptides or drugs molecules for specific tissue-type applications.[5,6] However, these approaches are limited by short half-life, low binding efficiency of the drugs or peptides, and inability to induce long-term therapeutic effects.[7] Hydrogels have also been used as a platform to support viral, nonviral and nanoparticle-based gene delivery systems. Encapsulating such gene delivery vectors inside hydrogels enables their controlled

* Address correspondence to alik@rics.bwh.harvard.edu.

Received for review April 15, 2014 and accepted July 2, 2014.

Published online July 02, 2014
10.1021/nn5020787

delivery at the desired site, preventing unwanted loss during the transit to the target site and allowing efficient localized gene therapy with reduced nonspecific spreading to other tissues. Thus, the hydrogel increases the local retention time of the vector at the target site, enhancing their chances of getting internalized by the tissues, which is currently a major limitation of nonviral nanoparticle-based delivery systems.[8] For example, it has been reported that alginate hydrogels, containing DNA−PEI aggregates, can enhance DNA uptake depending on the stiffness of the gel.[9]

Hydrogel/nanoparticle-based gene delivery system can be used to develop advanced bioactive hydrogels with tissue-specific functionalities. Such a system can efficiently deliver biotherapeutic molecules in a controlled and localized manner, as well as it can utilize the cell's own machinery for continuous and sustained production of the therapeutic protein, which is not possible with bulk protein delivery methods.[10,11] Studies so far have shown that mammalian viral gene delivery vectors, in combination with hydrogels, can be used for gene delivery applications.[12−15] However, nonviral vectors are clinically more attractive because of their advantageous features including superior biosafety profile, reduced risk of adverse immune reaction and negligible chance of viral gene integration to the host genome thereby zero risk of insertional mutagenesis.[16,17] A major disadvantage of nonviral nanoparticles compared to viral systems is poor transfection efficiency. It has been recently reported that graphene oxide (GO) nanosheets, a precursor of graphene, can be efficiently used to deliver genes efficiently when ionically bonded to cationic polymers such as PEI. PEI is known as a suitable material for gene transfer because it binds strongly to DNA, demonstrates proton sponge effects, and helps in escape of the delivered nucleic acids from endosomal/lysosomal pathways after cell internalization. Low molecular weight branched PEI is also known to have low cytotoxicity and can significantly enhance gene delivery efficiency in combination with GO.[18−21] This is mainly because of its unique delivery features such as suitable water dispersibility, high surface area and aspect ratio, efficient biomolecule loading and effective cell internalization properties.[22,23] In this regard, understanding the therapeutic potential of a hydrogel-based GO gene delivery system approach will be beneficial for enabling a range of therapeutic applications.

In this study, we have developed a low-modulus GelMA hydrogel, which is a chemically modified form of native gelatin protein. It was selected because of its biocompatibility, biodegradability and ability to support the formation of microvasculature and endothelial cord formation *in vitro* and *in vivo*.[24−27] This modified form of denatured collagen has the unique advantages of both natural and synthetic biomaterials. It retains the natural RGD-motifs of collagen that mediate cell attachment, while at the same time preserves the matrix degradation sites. Additionally, conjugation of gelatin with methacrylate groups helps to form photopolymerizable hydrogels with tunable mechanical and degradation properties. GelMA is also nontoxic to the cells when used under the optimal concentrations and degrees of methacrylation as reported in our earlier studies.[24,25] It has been previously demonstrated that GelMA can be microengineered to fabricate organized vasculature *in vitro*, support microvascular networks *in vivo* and support cardiomyocytes in a three-dimensional (3D) microenvironment when blended with carbon-based nanoparticles such as multiwalled carbon nanotubes (CNTs) and GO to generate mechanically strong, electroconductive hydrogels.[28−32] Here, GelMA has been impregnated with fGO nanosheets, for site-specific gene delivery of pro-angiogenic human vascular endothelial growth factor plasmid DNA ($pDNA_{VEGF}$) to damaged cardiac tissues. This injectable GelMA hydrogel (GG′), carrying fGO_{VEGF} ($pDNA_{VEGF}$ bound to fGO), was expected to induce a combinatorial effect, which would facilitate local myocardial neovascularisation at the injected sites, reduce fibrosis and potentially improve cardiac function in an *in vivo* model of acute myocardial infarction (AMI). Figure 1a illustrates the overall process of *in vitro* preparation of GelMA/fGO hydrogel-based hybrid gene delivery system and its *in vivo* localized administration in the heart for prolonged gene expression and therapy. The injectable GelMA matrix system would not only facilitate sustained supply of angiogenic genes to the myocardial tissues, but also provide protection of entrapped DNA against external harsh environment in the beating heart.

RESULTS AND DISCUSSION

Rheological Properties of the Formulated Hydrogel. To use the GO/GelMA nanocomposite hydrogels as an injectable gene delivery agent, the hydrogel should pass through surgical needles with minimum efforts. Moreover, after injection, the hydrogel should regain its mechanical properties and structural stability. To achieve such a clinically relevant material and facilitate easy release of fGO_{VEGF} nanosheets, here we used low degree methacrylation GelMA[24] whose injectability properties were evaluated by viscosity studies using rheometer and mechanical property analyzer.[31,33] The preliminary investigation using a 22-gauge needle indicates that all the nanocomposite hydrogel compositions can be easily injected (Figure 1b (inset)). For minimally invasive therapies, the hydrogels should be easily injected near the wound site and should have sufficient mechanical strength to withstand *in vivo* stresses. The ability of fGO/GelMA nanocomposites to flow under mechanical stress was determined by evaluating the shear thinning capability. In this, a

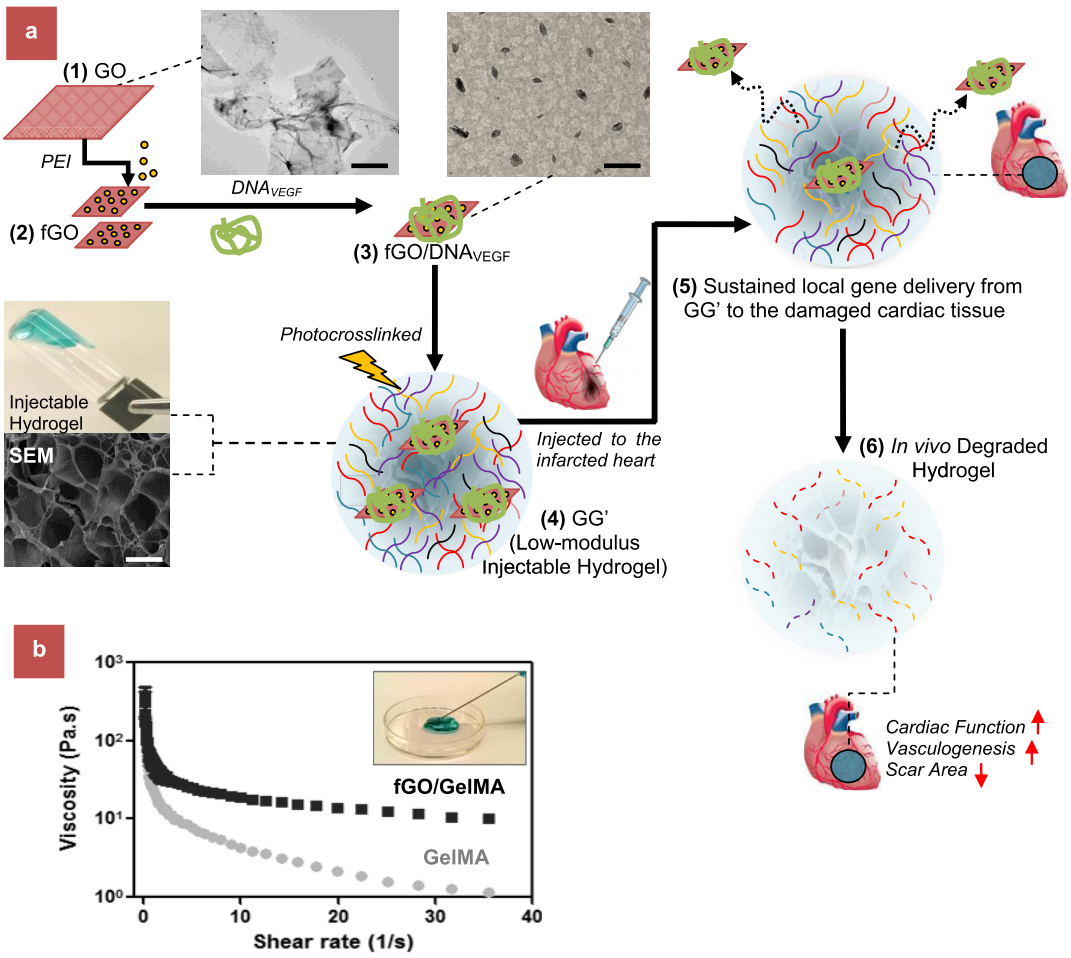

Figure 1. Preparation of injectable GG′ hydrogel for AMI therapy. (a) Schematic of stepwise formulation process of nanobioactive hydrogel and subsequent injection to treat damaged heart with acute myocardial infarction. (1) First, GO nanosheets are functionalized by amide bond with branched PEI to form cationic fGO. (2) fGO is then surface functionalized with anionic plasmids (DNA$_{VEGF}$) to form fGO/DNA$_{VEGF}$ as shown in TEM images. (3) These bioactive hybrids are then suspended in prepolymer of GelMA hydrogel and UV cross-linked under optimized condition to form (4) injectable fGO/DNA$_{VEGF}$ carrying GelMA hydrogel (GG′). (5) The latter is then intramyocardially injected in rat heart with acute intramyocardial infarction for local gene delivery of incorporated fGO/DNA$_{VEGF}$ nanocomplexes from GG′ hydrogel. (6) This eventually exhibits therapeutic effects by promoting myocardial vasculogenesis, which leads to reduced scar area and improved cardiac function. (b) Injectability of the developed GO carrying GelMA hydrogel. The viscosity of GO/GelMA nanocomposite hydrogels was monitored at different shear rates. At low shear rate, both fGO/GelMA and GelMA hydrogels had high viscosity. However, at higher shear rate, fGO/GelMA and GelMA hydrogels showed decreased viscosity. This indicates that both GelMA and fGO/GelMA were able to flow at higher shear rate and were easily injectable. The results also indicate that the addition of surface functionalized fGO to GelMA results in higher viscosity of fGO/GelMA at higher shear rate compared to GelMA. In other words, fGO reinforces the GelMA hydrogel network. Scale bar: 1 μm.

constant shear rate was applied to the hydrogel, and the viscosity was monitored. The decrease in the viscosity with increasing shear rate indicated that the nanocomposite hydrogels start flowing under mechanical stress. The results indicate that GelMA readily flows and the mechanical integrity is totally lost as the viscosity of GelMA was ~1 Pa. s at the shear rate of 50 s^{-1} (Figure 1b). The addition of fGO significantly increased the viscosity of the nanocomposite hydrogels at higher strain rate. This is mainly attributed to the physical interaction of surface functionalized fGO nanosheets, with GelMA. Moreover, with the addition of fGO to GelMA, mechanical strength of the hydrogel network was enhanced. This was also evident from the increase in storage modulus (G') and loss modulus (G'') of fGO/GelMA network in stress sweep, strain sweep and frequency sweep experiments compared to GelMA hydrogels (Figure S1). Overall, fGO/GelMA hydrogels were easily injectable using surgical needle, and the addition of fGO significantly reinforces the physical network of the nanocomposite hydrogels.

Characterization of the fGO/DNA Nanocomplex. Our main hypothesis was that an injectable hydrogel that induces localized gene therapy can significantly improve myocardial tissue repairing mechanisms. Recent works in small and large experimental animals have demonstrated that injectable hydrogels, comprising mainly native extracellular matrix (ECM), peptide-bound biopolymers, or myocardial ECM derived materials, can be effective in cardiac repair after infarction.[34−40] This is

because these hydrogels provide cardiac specific structural support, stimulate local healing mechanism, and generate bioactive products in the tissue microenvironment to promote endogenous stem cell homing. For instance, Ifkovits *et al.* demonstrated that mechanically tunable methacrylated hyaluronic acid hydrogels could be used as an injectable therapeutic biomaterial for healing of cardiac damage.[40] Similarly, it was postulated that the injectable GelMA hydrogel, comprised of natural biochemical cues, will be beneficial to the ischemic tissue that will potentially support vascular cell infiltration and endogenous repair mechanisms.

An important criterion while formulating an efficient gene delivery system is to establish a strong binding of negatively charged DNA to the surfaces of dispersed cationic fGO nanosheets. This was verified by transmission electron microscopy (TEM) confirming uniform nanostructure formation with good dispersivity, and zeta potential analysis confirming successful binding of fGO to pDNA (Figure 1a and Figure S2) following protocol mentioned elsewhere.[18] The TEM micrographs gave morphological evidence that the untreated GO (~5 μm) formed homogeneously dispersed nanocomplexes of around 30−40 nm dimensions after treatment and DNA binding. Zeta potential analysis at physiological pH 7.4 showed that the untreated pristine GO was negatively charged with a zeta potential of -37 ± 2.4 mV. On the other hand, fGO showed a highly positive charge (43.0 ± 3.2 mV). The positive zeta potential value of fGO, upon binding with the negatively charged pDNA, was reduced. The resulting zeta potential values depended on the N/P ratios, where N/P stands for the ratio of moles of the amine groups of cationic PEI polymer to those of the DNA phosphates. N/P ratio of 16, represented as fGO $(16)_{VEGF}$, showed highest zeta potential (15.8 ± 3.5 mV), while at N/P ratio of 4 the charge decreased to negative value because of overloaded pDNA on fGO surfaces. This result confirmed the efficient hybrid complex formation, generated by strong electrostatic interactions of plasmid DNA with fGO nanosheets under optimized condition as reported elsewhere.[18] The MTS tetrazolium cytotoxicity assay (Promega, Madison, WI) of fGO nanocomplexes with embryonic rat cardiomyocytes (H9c2 cells, ATCC) confirmed that fGO (N/P ratios ranging from 4 to 16) did not invoke statistically significant cytotoxic effects on the H9c2 cells compared to untreated control (Figure S3).

***In Vitro* Gene Delivery of the Hydrogel.** To prepare the gene delivery system, fGO_{VEGF} was dispersed by vortexing in 5% GelMA prepolymer solution and the prepolymer mixture was photo-cross-linked under optimized UV exposure based on previously established protocol, to form low modulus injectable hydrogel.[31] To confirm the release of fGO_{VEGF} nanocomplexes from the hydrogel, the latter was incubated in phosphate buffer saline (PBS) solution for 72 h and samples were collected in regular intervals for agarose gel electrophoretic run (Figure S4A). The detected band intensities for different time points in the gel confirm slow release of pDNA from GelMA over 72 h, while the retention of these bands within the wells of the agarose gel confirms that pDNA was still bound to the fGO that led to the retardation of electromobility shift of the bound pDNA, similar to other studies.[18,21] This was followed by transfection of the cardiomyocytes with the eluted fGO_{GFP}, carrying green fluorescent protein (GFP) gene, or fGO_{VEGF} nanocomplexes from the GelMA hydrogels, where fGO $(16)_{GFP}$ showed highest transfection efficiency (Figure S4B). The release profile of VEGF protein in conditioned media (CM) from fGO $(16)_{VEGF}$ transfected H9c2 cardiomyocytes showed rapid overexpression of the growth factor in the first 4 days post-transfection as quantified by ELISA, while it gradually decreased over time by day 14 (Figure S4C). The data also reconfirmed that GG′ group can significantly enhance the gene delivery efficiency compared to GG (GelMA with free $pDNA_{VEGF}$) and control G (only GelMA) groups.

***In Vitro* Pro-Angiogenic Activities of the Hydrogel.** The bioactivities of the released VEGF by GG′ group were evaluated *in vitro* by investigating the proliferative capacity of the human umbilical vein endothelial cells (HUVECs) in 3D culture in high degree methacrylated (~80%) GelMA hydrogel. MTS assay was used to assess the proliferation potential of HUVECs treated with CM (containing VEGF secreted by H9c2) from experimental samples.[41] The results were illustrated as percent increase in HUVEC proliferation relative to that induced by CM from unstimulated control group (taken as 100%). As shown in Figure 2a (i), CM from group GG′ showed highest HUVEC proliferation ($133.9 \pm 6.0\%$) compared to GG′ + Ab and Control (Nontreated) groups. This is because the overexpressed VEGF from H9c2 cardiomyocytes was neutralized with antibodies in GG′ + Ab group. This proliferation rate was directly dependent on the amount of the VEGF released which explains why the treated group demonstrated better results than nontreated Control and GG′ + Ab groups. The lower left panel in Figure 2a (ii) represents the calcein stained HUVECs in 3D hydrogel in different groups. Interestingly, the GG′ group also showed sprouting of HUVECs in the hydrogel which was absent in other groups. Furthermore, we tested the ability of CMs from different groups to increase HUVEC wound healing in a 2D monolayer as demonstrated in other studies.[42] As depicted in Figure 2b (i) and the corresponding representative pictures in lower right panel in Figure 2b (ii), stimulation of wounded HUVEC monolayer with CM from GG′ induced significant healing of wound area ($25.6 \pm 3.1\%$) compared to CM from unstimulated control ($5.4 \pm 0.7\%$) and GG′+Ab group ($2.5 \pm 0.1\%$). Preincubation of CM with the neutralizing anti-VEGF antibodies completely hindered VEGF

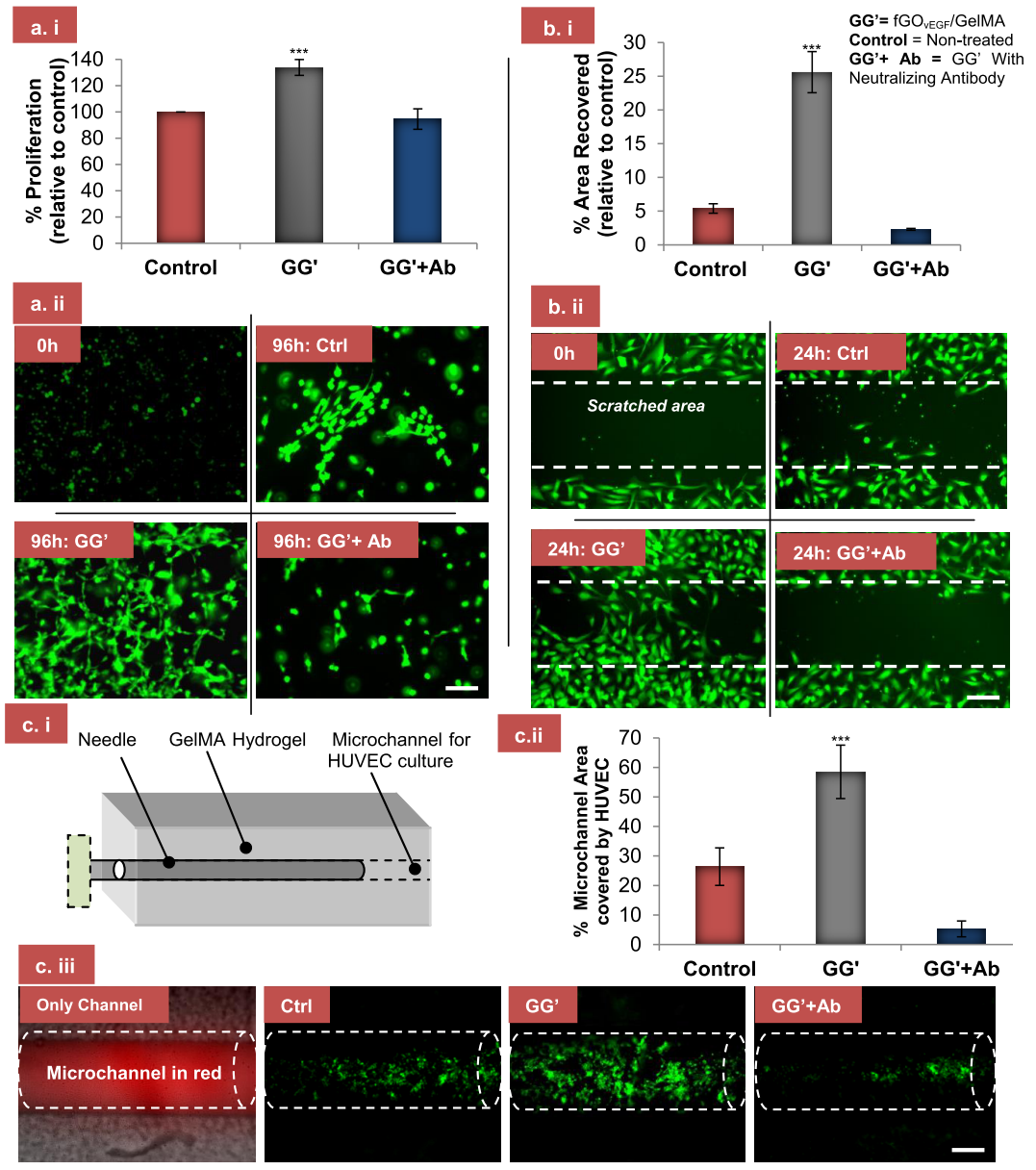

Figure 2. *In vitro* **functionalities of GG′ hydrogel on HUVECs. (a i and ii) Proliferation of HUVECs in 3D, grown in the presence of conditioned media (CM, with or without excess of neutralizing anti-VEGF antibodies, Ab: 1 mg/mL) from fGO/DNA$_{VEGF}$/GelMA transfected H9c2 cardiomyocytes. As control group, CM from nontreated cells was taken. A total of 50 μL of GelMA prepolymer containing HUVECs were added per well in 96 well-plate. After photo-cross-linking was performed, the cell containing gels were grown in different CMs for 96*h*. Cell proliferations were detected by MTS colorimetric assay, while data (n = 3) presented in graph were normalized by that from control group. Lower left panel shows the representative photomicrographs of each group where HUVECs were stained with calcein dye. Interestingly, HUVEC in GG′ group, apart from inducing significant proliferation, also demonstrated highly branched tube-like structure formation absent in other groups. (b i and ii) VEGF-induced migration of HUVECs in wound healing scratch assay. HUVEC monolayer was wounded with cell scraper and treated with CM from different groups. HUVECs were photographed 12 h post-treatment (lower panel) and the percentage of scratched area (which was initially free of cells, marked by the white dotted border lines) covered by the migrated cells were analyzed using ImageJ software. (c i–iii) To confirm the potential of CM in combination with GelMA biomaterial to produce vascularized microstuctures, HUVEC adhesion and migration assay inside GelMA (highly methacrylated) microchannels was performed. The microchannel was made by needle (200 μm) insertions and photo-cross-linking. In all groups, HUVECs were suspended in CM from individual groups and seeded inside the microchannel. After 24 h, photomicrographs of the cell cultured microchannels (lower panel) were taken and analyzed for percentage of microchannel area covered by adhered and migrated HUVECs in different experimental groups. Data are expressed as mean value ± standard deviation (SD). ***P < 0.001, n = 3. Scale bar: 100 μm.**

induced wound healing, clearly suggesting that chemotactic signals from VEGF enhances the wound healing effect. In addition, we explored whether CM can also induce HUVEC attachment and spreading in a hydrogel-based channel system within restricted microenvironment. As described in earlier studies, a microchannel was formed inside GelMA hydrogel (high degree methacrylate) and 5 × 10^6 HUVECs/mL

was grown inside the microchannel in the presence of CM from different groups.[24] Twenty-four hours post incubation with CM from different groups demonstrate that GG′ group had significantly higher HUVEC attachment and spreading inside the microchannel compared to GG (Figure 2c: 58.5 ± 9.1% *vs* 26.4 ± 6.4%). These data confirmed the proliferative, wound healing and chemotactic effects of VEGF, secreted from GG′, transfected H9c2 cells.

***In Vivo* Biocompatibility of fGO/GelMA Hydrogel.** Despite the multiple clinical trials and growing understanding in cardiovascular research, clinical outcomes of currently available AMI treatments are deeply influenced by the post AMI complications, such as inflammation, stent thrombosis, and other life threatening cardiovascular risk factors.[43−45] However, promoting vascularization at the injured site to reduce scar formation and ventricular remodeling has been considered as a viable treatment method, as observed in several gene therapy studies with viral vectors.[13,42,46,47] Through this study, we intended to develop a biocompatible, nonviral, controlled gene delivery system using hydrogel-based cationic GO for AMI therapy. Recently, it has been demonstrated that GO nanosheets support and maintain cardiomyocyte functionalities when cultured *in vitro* in combination with GelMA hydrogel.[31] Taking advantage of the complementary strengths of GO, such as relatively high therapeutics loading capacity, low immunogenicity and high gene delivery efficiency,[18,21] along with microvascular network supporting properties of biodegradable GelMA hydrogel,[24,25] here we developed fGO_{VEGF} carrying injectable GelMA hydrogel and hypothesized that it will be able to successfully treat AMI *in vivo*.

As establishing the *in vivo* biocompatibility of the formulated GO-based hydrogel is of paramount importance, building on the *in vitro* results, here we investigated its inflammatory effects in immunocompetent rat model with AMI. The AMI was induced in the rat models by occlusion of the left anterior descending coronary artery according to established laboratory procedures.[42] Subsequently, 300 μL of injectable hybrid hydrogels was intramyocardially injected at three different sites in the peri-infarct regions of the heart (Figure 3a). One group received fGO suspended in 5% GelMA hydrogel (G_t, $n = 3$) and the control sham group received only similar infarction (G_c, $n = 3$). Seven days post injection, the formalin fixed paraffin embedded tissue sections, specifically from the injected regions, were isolated using laser capture microscopy (LCM).[48] This was followed by total RNA extraction for quantitative analysis of four different miRNAs, and detection of the changes in inflammatory marker expression compared to untreated control. The miRNAs are small, noncoding RNA molecules (~20 nucleotides) present in introns and exons of noncoding transcripts and can influence transcriptional regulators, cytokines and cell surface receptors, thereby affecting the entire inflammation and immune response system.[49,50] The markers chosen for the study include miRNAs for proinflammatory role (miR-155), inflammation resolution role (miR-146a), cardiac aging and function (miR-34a) and cardioprotective role under apoptotic condition (miR-145).[51−53] Quantitative PCR (qPCR) analysis showed no significant differences between control and tested animals for all the four miRNAs analyzed in the study (Figure 3b). Similar results were obtained by ELISA analysis of pro-inflammatory tumor necrosis factor α (TNFα) and anti-inflammatory interleukin-10 (IL10) cytokines in blood plasma where no significant differences were detected in the ratio of pro/anti-inflammatory cytokines between fGO/GelMA and control group (Figure 3c). Similar observations were reported in a recent study by Chowdhury *et al.* where the group used dextran functionalized graphene nanoplatelets to assess the hematological and inflammatory responses *in vivo*.[54] Concomitantly, this trend was noticed by immunostaining myocardial tissue sections for TNFα expression (Figure 3d) and hematoxylin and eosin (H&E) staining (Figure 3e) to assess acute inflammatory cell infiltration to the inflammatory site. These data confirmed that the combination of GO and GelMA did not invoke any significant toxicity or inflammatory response *in vivo*.

***In Vivo* Therapeutic Efficacy in Myocardially Infarcted Rat Model.** After confirming *in vivo* biocompatibility, we evaluated the *in vivo* therapeutic efficacy of the fGO_{VEGF} based hydrogel in rat model with AMI using established analysis methods.[13,42,46,47] At first, the gene delivery efficiency was confirmed by fGO_{LacZ}/GelMA (Figure 4a), where Lac Z was used as the β-galactosidase coding reporter gene to trace the protein expression in the transfected heart tissue. This was confirmed 7 days post operation, by the localized 5-bromo-4-chloro-3-indolyl-β-D-galacto-pyranoside (X-gal) staining of the myocardial tissue at the injected sites (Figure 4b,c). The analysis of the X-gal-stained heart revealed that the LacZ gene expression was mainly limited to the injected regions surrounding the infarct region as indicated by the blue X-gal staining. In a similar way, to achieve highly localized transfection and angiogenic effects in myocardial tissue, injectable GelMA carrying fGO_{VEGF} hydrogels were administered via direct intramyocardial injections at the peri-infarct region post infarction. It was postulated that the strong angiogenic effect of the hydrogel would help in promoting vasculogenesis, reducing scar area formation and improving the heart function in treatment groups. Toward this goal, a total of 28 immunocompetent rats were used for *in vivo* efficacy experiment (Groups: GG′ = fGO_{VEGF}/GelMA; GG = DNA_{VEGF}/GelMA; G = GelMA, control = nontreated; n=7). The neovasculature formation in the peri-infarct area was assessed by detecting the capillary (Figure 4d) and artery densities

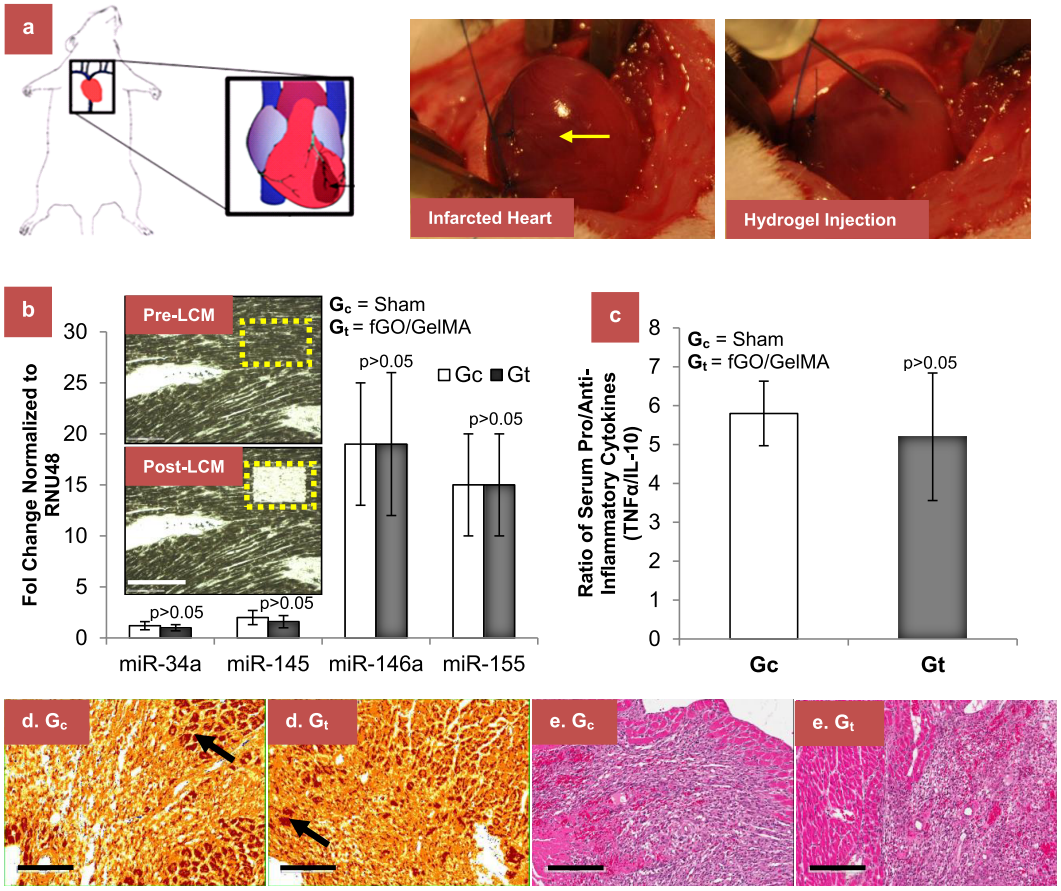

Figure 3. ***In vivo*** **delivery and biocompatibility of injectable fGO carrying GelMA. (a) Schematic of rat heart with AMI. Photograph (infarcted heart) represents a myocardially infarcted rat heart after causing myocardial infarction by ligation of left anterior descending artery. Arrows indicate the damaged area in the left ventricular region. Photograph (hydrogel injection) shows the route of administration** ***via*** **direct intramyocardial delivery of injectable fGO/GelMA hydrogel to the peri-infarct zones. (b) Representative pictures of peri-infarct region of ventricular tissues 7 days post injection, pre- and postlaser capture microdissection (LCM) (scale bar: 100 μm). Post-LCM tissue capture and RNA extraction and qPCR based miRNA expression assays were performed to compare the inflammatory marker-specific miRNA levels in Sham and fGO/GelMA hydrogel treated groups. The data in graph represents fold change in expression levels of inflammation-specific miRNAs, miR-34a, miR-145, miR-146a and miR-155, between the two groups normalized to RNU48, an abundant and stable human small nuclear RNAs (snRNAs). No significant differences were found between the two groups confirming the** ***in vivo*** **biocompatibility of the injected hydrogels. (c) Quantification of blood plasma TNFα and IL10 represented as a ratio of pro and anti-inflammatory cytokines analyzed by ELISA assay ($P < 0.05$ = statistically significant, $n = 3$). (d and e) fGO/GelMA hydrogel does not invoke any significant difference in pro-inflammatory TNFα expression or white blood cell accumulation in the infarcted heart compared to sham control. The tissues were either immunostained with TNFα antibody to trace myocardial TNFα expression (d) or counterstained with H&E (e) to demonstrate histological morphology of orderly arranged myocardial cells The TNFα immunoreactive cells were stained as dark brown color. Data are expressed as mean value ± SD. Scale bar: 200 μm.**

(Figure 4e). For this, immunohistochemical staining was performed with antibodies against (platelet endothelial cell adhesion molecule-1) PECAM-1 for identification of HUVECs and smooth muscle α-actin for tracing the smooth muscle cells. As shown in Figure 4d, significant improvements were observed in capillary density in the GG′ compared to other groups (148.7 ± 21.2/mm^2 for GG′, 115.6 ± 8.4/mm^2 for GG *vs* 118.0 ± 17.4/mm^2 for G, 94.5 ± 15.2 for untreated control, $p < 0.001$) analyzed by immunostaining against PECAM endothelial marker (Figure S5A). This indicates that the treatment group was able to induce neoangiogenesis in a paracrine way by releasing VEGF angiogenic factors to stimulate localized vessel sprouting through improved paracrine VEGF secretion. However, no significant differences in arteriole densities ($p > 0.05$) were found between the groups as reported in Figure 4e and Figure S5B with smooth muscle α-actin staining. Histomorphometric analysis of sirius red stained heart sections confirmed that the treatment helped to attenuate scar area formation (Figure 5a,b: 19.4 ± 5.8% for GG′, 28.1 ± 4.2% for GG *vs* 27.5 ± 7.7% for G, 35.6 ± 4.2% for control, $p < 0.01$). This data is in support of earlier studies, which showed that increment in blood vessel density could support reduction of scar formation.[42,46,47] GG′ group also significantly reduced the fibrotic area compared to GG as observed from ventricular infarct area analysis. To investigate if the reduction in scar formation improved heart function, the cardiac ejection fraction percentage (EF%) at

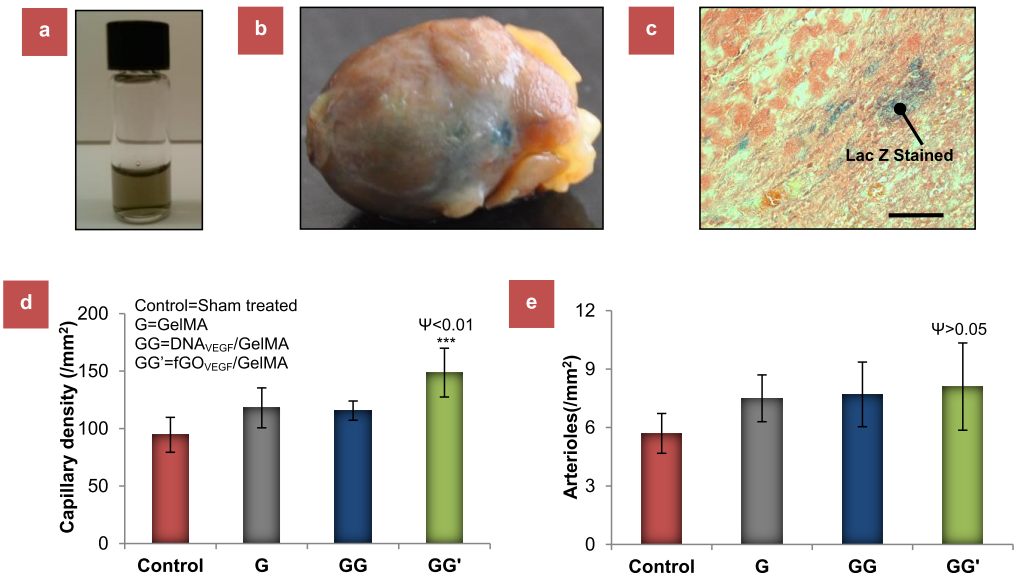

Figure 4. Confirmation of *in vivo* gene delivery and pro-angiogenic effects of GG′ hydrogel for AMI therapy. To confirm the gene delivery potential of formulated hydrogel, fGO$_{Lacz}$/GelMA was injected intramyocardially and expressions of Lac Z reporter genes in the heart regions were confirmed. (a) Injectable nanobioactive hydrogel. (b) Image of explanted rat heart showing Lac Z gene expression by X-Gal staining (in blue color) and (c) ventricular tissue section in histology slide at microscopic level. Quantification of (d) capillaries and (e) arteriole densities in the peri-infarct region, 14 days post injection of VEGF therapeutic genes in group GG′, GG, G and control (with sham treatment after infarction) by immunohistological staining of CD31 and smooth muscle α-actin. Data are expressed as mean value ± SD. ANOVA statistical analysis with Bonferroni post hoc test was performed to determine the significance of the experiments. $p < 0.0001$; ***$P < 0.001$, **$P < 0.01$, *$P < 0.05$ *vs* time-matched control ($n = 7$). P values comparing time-matched GG′ and GG are indicated by ψ. Scale bar: 100 μm.

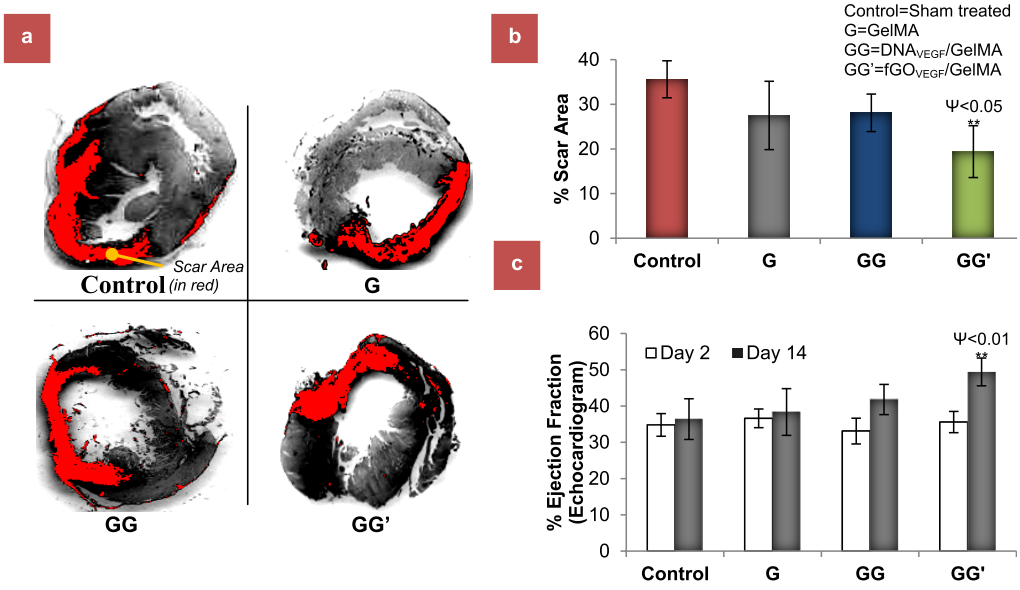

Figure 5. Assessment of *in vivo* scar areas and cardiac functions of infarcted hearts treated with GG′ hydrogel therapy. (a and b) Scar area determination by morphometric analysis of the left ventricle in different groups. Representative images of left ventricle myocardial sections stained with Sirius red show the cardiac fibrosis regions (in red). Sham operated and untreated infarcted group were used as controls. The red area represents ECM deposition in the scar tissue and the gray area represents the myocardium. (c) Echocardiographic assessment of cardiac function. For this, heart ejection fraction (EF%) was monitored at day 2 and 14 post treatment. GG′ showed significantly better EF% than other groups. Data are expressed as mean value ± SD. ANOVA statistical analysis with Bonferroni post-hoc test was performed to determine the significance of the experiments. $p < 0.0001$; ***$P < 0.001$, **$P < 0.01$, *$P < 0.05$ *vs* time-matched control ($n = 7$). *P*-values comparing time-matched GG′ and GG are indicated by ψ.

different time periods (day 3 and 14) were monitored using echocardiography.[42,46] EF% of all of the groups was around 30% (baseline) on day 3 post infarction, indicating successful AMI in all groups. As presented in Figure 5c, significant improvement was observed in EF% of GG′ group compared to other experimental groups by day 14 (49.4 ± 3.8% for GG′ *vs* 41.8 ± 4.2% for GG *vs* 38.4 ± 6.4% for G *vs* 36.4 ± 5.6% for control, $p < 0.01$).

CONCLUSIONS

In summary, this new gene-activated hybrid material promises new advancement in AMI therapy to meet the current clinical needs. The study not only confirms the *in vivo* efficacy of the developed hydrogel for post-AMI therapy but also provides insights into the biocompatibility aspects of the system. This strategy is particularly advantageous compared to widely studied stem cell therapy whose application is limited mostly by frequent immune rejections by patients, maintenance of cell viability and retention at the target site, chances of teratoma formation, along with plethora of ethical, logistical and technical challenges for cell isolation and culturing. Moreover the fGO-based hydrogel was characterized by scanning electron microscopy, rheological property testing and zeta-potential analysis. These tests confirmed suitable injectability and DNA adhesion properties of the fGO-based hydrogel formulation. Collectively, the study underscores the potential of this hydrogel-based, nonviral gene delivery system which can effectively transfer genes *in vivo* as well as induce sustained therapeutic effects. The formulation is simple and can be easily applied to plasmid DNA and other nucleic acid delivery systems for site-specific treatment of different diseases. The strategy can also limit the number of doses necessary for long-term effects, compared to the bolus doses of active protein or drug molecules. Such GO-based gene delivery approach can also be useful to direct cell behavior in well-defined 3D hydrogel microenvironment system for advanced tissue engineering applications. In fact, the delivery of genes using fGO can function not only as gene complexing agents but also as structural scaffolds for tissue engineering. This combination of GO/DNA therapy and tissue engineering within a single system can be a new strategy for regenerative medicine.

Although the study findings exemplify the beneficial effects of low modulus hydrogel-based gene therapy treatment, further studies are needed to elucidate the long-term effects of the treatment on heart function. It is important to investigate whether multiple administration of the therapy will invoke further salutary effects to the infarcted heart. To our advantage, the GelMA/GO hydrogel based gene delivery system can be potentially used for codelivery of multiple therapeutic genes, bioactive small molecules and peptides. Slow delivery of combination of such therapeutics within the same formulation may augment the protein expression or biofunctional activities of the delivered materials. Another crucial factor that needs further studies is to understand the long-term fate of GO in the host system. Studies in this direction have demonstrated that polymer functionalized GO remains in the host body for a long time postadministration, but it does not significantly invoke the *in vivo* toxicity.[55,56] However, intravenous administration of GO nanoflakes in mice in high concentration (4 mg/kg) for 5 consecutive days induced mutagenesis.[57] Also, Qu *et al.* reported GO can increase the level of reactive oxygen species in macrophages, triggering drastic cell morphologic changes and eventual *in vitro* necrosis.[58] Thus, special considerations have to be given while optimizing the *in vivo* dosages and characterizing the stability of surface functionalized GO nanosheets to ensure their long-term biocompatibility and safety.

Taken together, this study demonstrated the postulation that this newly formulated gene-active GO/GelMA hydrogel can take advantage of the unique features associated with GelMA hydrogel and GO-based angiogenic gene delivery system to exhibit enhanced AMI therapeutic efficacy without any significant side effects. In particular, the injectable nanocomposite hydrogels induced *in vivo* beneficial effects on tissue revascularization at injured site and improved contractile performance, as corroborated by vasculogenesis, scar area analysis and echocardiogram data examinations. The findings from this study also provide insight into the biocompatibility properties of this new therapeutic delivery system for cardiac applications.

MATERIALS AND METHODS

Preparation of Injectable GelMA Hydrogel Carrying GO/DNA Nanocomplex. *Preparation of Hydrogel.* Low methacrylated GelMA was synthesized as reported earlier.[24] Briefly, gelatin at 10% (w/v) was added in PBS at 50 °C and stirred for 1 h to completely dissolve it. While stirring, methacrylate anhydride (MA) was added dropwise (0.25% vol %) to the gelatin solution. After 2 h, the reaction was stopped by diluting the solution with PBS. The diluted mixture was dialyzed against distilled water with a dialysis membrane (M_w cutoff of 12−14 kDa) for 7 days to remove unreacted MA and salts. The resulting solution was subsequently frozen in liquid nitrogen and lyophilized to obtain the final product (~20% methacrylation).

Preparation of GO/DNA Nanocomplex Formation. GO nanosheets were purchased from Nanocs, Inc. and functionalized to low molecular weight branched PEI using method used elsewhere.[18] Briefly, to bind low molecular weight PEI (M_w = 1.8 kDa) to the carboxyl groups of GO by 1-ethyl-3-[3-(dimethylamino)propyl]carbodiimide hydrochloride (EDC)/*N*-hydroxysuccinimide (NHS) coupling, GOs were suspended in deionized water by sonication, and EDC and NHS were added to the GO solution (0.5 mg/mL, 1 mL). Then, 100 μL of triethylamine was added to a PEI solution in deionized water. The PEI solution was added to the GO prepared (1 mL, 0.5 mg/mL) and stirred for 24 h. The resulting PEI−GO solution was dialyzed against a 3.5 kDa cutoff dialysis membrane for 48 h to get rid of the unreacted components. The surface charge of GO, PEI−GO (fGO), and PEI−GO/DNA (fGO_{DNA}) complexes with different N/P ratios in PBS buffer were confirmed by zeta potential measurements using Zeta Potential Analyzer (Brookhaven Instruments Corporation, Holtsville, NY). fGO_{DNA} nanocomplexes were prepared at various N/P ratios by the addition of fGO suspensions to the plasmid DNA solutions in PBS buffer. For the study, plasmid DNAs, carrying either $VEGF_{165}$ (Origene) or GFP expressing genes (Promega) driven by a cytomegalo-virus (CMV)

immediate early promoter, were used as described in earlier studies.[13,42] The final plasmid DNA concentration was adjusted to 33 μg/mL, and the mixtures were incubated for 30 min to form the electrostatic nanocomplexes (fGO_{GFP} or fGO_{VEGF}) prior to measurement of the zeta potential. Transmission electron microscopy (TEM) was used to obtain the size characterization. The nanocomplexes were suspended in PBS and analyzed on CM200 FEG-TEM (Philips, Markham, Ontario, Canada).

Preparation of fGO/GelMA Hydrogel. Lyophilized GelMA (5 wt %) and photoinitiator (0.25 wt %), 2-hydroxy-1-(4-(hydroxyethoxy)phenyl)-2-methyl-1-propanone (Irgacure 2959; CIBA chemical) were first dissolved in PBS at 80 °C for 30 min. Then, 75 μL of this prepolymer solution, along with fGO_{VEGF} (16), was pipetted into the space between two glass slides separated by a 1 mm spacer and exposed to UV at 6.9 mW/cm^2 (wavelength 360−480 nm) for 15 s similar to the method used earlier.[34] The compressive modulus and rheological properties of the formed hydrogel was analyzed using Instron 5524 mechanical analyzer (Instron, Canton, MA) and AR-G2 Rheometer (TA Instruments) respectively.[33,43]

***In Vitro* Cardiomyocyte Transfection and Biofunctional Analysis.** *Cytotoxicity Assay.* First, the *in vitro* cytotoxicity of the different fGO formulations was analyzed using MTS cell proliferation assay (Promega) according the manufacturer's instructions.[41] This was followed by release kinetics study of fGO/DNA nanocomplexes from entrapped GelMA over time. The data confirmed rapid release of the entrapped fGO/DNA nanocomplexes from the GelMA hydrogel in physiological solution as detected by gel retardation assay. The experiment was performed also to confirm the successful binding of fGO with DNA molecules where the DNA bound nanocomplexes show retardation in gel electrophoresis.

Cardiomyocyte Transfection Study. To optimize the transfection efficiency, gene delivery efficiency of fGO_{GFP} with three different N/P ratios (4, 8, 16), control GO and positive control PEI/DNA_{GFP} groups were studied, where N/P is the ratio of moles of the amine groups of cationic PEI to those of the phosphate ones of DNA. To do this, fGO_{GFP} nanocomplexes, eluted from GelMA hydrogel, were used for the transfection study. Initially, the H9c2 cells were seeded in 24-well plate at 10^5 cells/well. Then, the 72 h eluted samples, adjusted to 2 μg plasmid DNA_{GFP} per 50 μL of fGO/DNA_{GFP} solution, were added to the 250 μL of serum-free culture medium and the mixture was incubated for 4 h according to earlier established protocol.[18] The media was then replaced with 500 μL of fresh culture medium containing 10% fetal bovine serum (FBS) and grown in 37 °C humidified incubator at 5% CO_2. After 4 days, photomicrographs of transfected H9c2 cells using fluorescence microscope (Nikon Eclipse TE2000-U) were taken under 5 different fields per sample and percentage transfected cells was calculated. As we obtained best results with fGO_{GFP} (16) group, we did further studies with fGO_{VEGF} (16) group. Similar to the above method, the eluted fGO_{VEGF} (16) were added to H9c2 cells and the conditioned media (CM) were collected at regular time points for 14 days and analyzed for VEGF ELISA (R&D Systems) following manufacturer's protocol.

HUVEC Cell Proliferation Assay. To investigate the bioactivity of released VEGF on HUVECs, Day 4 CMs from three groups (control = nontreated, GG′ = fGO_{VEGF}/GelMA, GG′ + Ab = GG′ with VEGF Antibody) were collected. In GG′ + Ab, the CM was preincubated with anti-VEGF neutralizing antibody (R&D Systems; 1 mg/mL) for 30 min, before adding to the cells. For the HUVEC cell proliferation assay in 3D, 50 μL of 3×10^6 HUVEC/mL of GelMA prepolymers was added per well in triplicate for each sample in 96-well plates and photo-cross-linked using standard method.[28] After 12 h of culturing in serum starved condition (1% FBS), the cells were washed twice with PBS and 200 μL of conditioned media from different groups with and without anti-VEGF antibody supplementation was added to the corresponding set of wells. After 96 h, the absorbance was measured at 490 nm using cell proliferation assay (Cell Titer 96 Aqueous Non-Radioactive Assay, Promega) in a plate reader. In a separate group, the cells were stained with calcein dye to track the viable cells.

HUVEC scratch assay. To check the wound healing potential of released VEGF, HUVECs were seeded into 24-well plates and grown to confluency. After 24 h of serum starvation (1% FBS), lesions were made in the monolayer using cell scraper.[42] Cells were rinsed with PBS, and then incubated with the H9c2 CM from different experimental groups (GG′, control, GG′ + Ab) for 24 h. Cells were fixed with 4% paraformaldehyde after 24 h and the number of cells which had moved across the starting scratched lines were measured for all groups. Three fields were analyzed for each well.

HUVEC Migration through Microchannel. To demonstrate the potential of CM for GelMA based vascularised tissue engineering, HUVECs were seeded into a perfusable GelMA microchannel. For this, a block of GelMA was photopolymerized containing a syringe needle, which when removed contained a 200 μm diameter perfusable channel as shown in Figure 3. Rhodamine-bound dextran (200 kDa) was perfused through the microchannel to demonstrate the ability to create perfusable, microfluidic channels within the GelMA microstructures. This was followed by addition of 5×10^6 HUVEC/mL of CM media from different groups into the microchannel and the cultures were grown for 24 h in normal cell culture condition. Then, the cells were stained with calcein dye, stained, photographed under fluorescence microscope, and analyzed by ImageJ for percentage of channel area covered by HUVEC.

Induction of Myocardial Infarction in Rat Model for *in Vivo* Studies. Immunocompetent Lewis rats (200−250 g, Charles River, QC) were used in an *in vivo* myocardial infarction model according to established protocols.[13,42] All procedures were in compliance with the Guide for the Care and Use of Laboratory Animals (NIH publication No. 85-23) and the Guide to the Care and Use of Experimental Animals of the Canadian Council on Animal Care. Briefly, Lewis rats were anesthetized using isoflurane followed and mechanical ventilation (Harvard Ventilator, Canada) using catheter at 80 breaths/min. Anesthesia was maintained with 3% isoflurane. The left coronary artery was ligated 2 mm from its origin with polypropylene suture. Fifteen minutes post ligations of the arteries, the rats with acute myocardial injections were subjected to treatments with different formulations. For the experiments, 300 μL of injectable GO carrying GelMA hydrogel with different formulations was used. Three equal left ventricular direct intramyocardial injections, 100 μL each, were injected at the peri-infarct regions.

Investigating the *in Vivo* Biocompatibility of fGO/GelMA Hydrogel. To confirm the biocompatibility of the developed hydrogel, animals were divided into 2 groups. One group of animals, after myocardial infarction, were injected with 300 μL of fGO/GelMA containing 0.5 mg fGO/mL GelMA (G_t, n = 3) and the other control group received only PBS solution (G_c, n = 3). Seven days post injection, the animals were sacrificed. The excised hearts were immediately soaked in cold saline to remove excess blood from the ventricles and fixed in neutral-buffered 4% formalin. The samples were embedded in paraffin and sectioned at 5−6 μm thick for histological (H&E) and immunostaining (myocardial TNFα staining) analysis.

To enable quantitative PCR (qPCR) based microRNA analysis selected ventricular region laser capture microdissection (LCM) instrument was used. First, a rectangular areas measuring ~5000 μm^2 in the peri-infarct regions of the heart sections were carefully dissected out using PALM Laser system (Carl Zeiss) from each group.[48] The captured tissues were immediately lysed in Trizol (Invitrogen). Then the tissue was processed for miRNA isolation. To do this, total RNA was extracted from all the samples using Trizol RNAeasy mini (Qiagen) kit protocols. Total RNA was reverse transcribed using Taqman miRNA RT (reverse transcription) kit, muliplexed for all the miRNA RT primers included in the study. The resultant complementary DNAs (cDNAs) were subjected to a preamplification PCR using multiplexed miRNA probes. The amplified products were then used for the final qPCR for the individual miRNAs. Relative expression of each miRNA was calculated using ΔΔCt method, normalized to RNU48 (an abundant and stable small nuclear RNA) expression.[48]

In addition, the cardiac blood was also collected to investigate the plasma inflammatory cytokine profile using rat IL10 and TNFα ELISA kit (SA Biosciences) using manufacturer's protocol.

Assessment of *in Vivo* Therapeutic Efficacy of the Developed GO/DNA Based Hydrogel. *Confirmation of in Vivo Gene Delivery.* To confirm the *in vivo* gene delivery to the myocardial tissue using GelMA based GO gene delivery system, 3 animals were intramyocardially injected with fGO_{LacZ}/GelMA hydrogel. *In vivo* Lac Z expression at the injection sites was detected using X-gal (bromo-chloro-indolyl-galactopyranoside) by sacrificing the animals 7 days post administration as previously described.[42]

Confirmation of Functional Efficacy. To perform this, myocardially infarcted rats were divided into 4 groups. The G group ($n = 7$) received 300 μL of only GelMA, GG group ($n = 7$) received DNA_{VEGF}/GelMA and GG′ group ($n = 7$) received fGO_{VEGF}/GelMA (N/P ratio 16), where the last 2 groups received 20 μg of plasmids per animal following the protocol mentioned above. The control group received 300 μL of PBS only. To understand the functional efficacy of the different treatment groups, animals were analyzed by (a) immunohistochemistry to examine neovascularisation, (b) histological analysis to detect scar area, and (c) echocardiography to examine cardiac performance 2 weeks post treatment.

(a) Immunohistochemistry to detect neovascularisation: Capillary and arteriole densities in the peri-infarct regions were quantified by tracing neovascularized regions. Immunohistochemical staining was performed with anti-PECAM1 (Santa Cruz Biotechnology, Santa Cruz, CA) and smooth muscle α- actin antibodies to trace the vascularized myocardial tissues in the peri-infarct regions. For capillary density measurement, five fields in the peri-infarct regions were imaged and capillaries with less than 10 μm diameter were counted. The capillary densities were quantified as the mean of total PECAM-positive microvessels per mm^2 area using three different fields of the per-infarct tissue regions per animal. In a similar way, arteriole densities were quantified as the mean of total smooth muscle α-actin positive microvessels per mm^2 area for each group of animals.

(b) Histological analysis of scar areas: Paraffin embedded 5 μm thickness samples were deparaffinized and stained with collagen-specific Sirius Red dye for detection and quantification of fibrosis areas (in red) in the ventricular region using ImageJ-1.41 software as reported earlier.[59]

(c) Echocardiography for cardiac performance evaluation: Transthoracic echocardiography studies were performed using echocardiographic instrument (Sonosite, Seattle, WA) after sedating the animals with isoflurane. Left ventricular ejection fractions (EF) were calculated from the echocardiogram in all the four groups 2 days (baseline) and 2 weeks post infarction.[59]

Statistical Analysis. Quantitative variables are presented as mean ± standard deviation (SD) from independent experiments as described in the figure legends. Statistics were performed using two-way and/or one-way analysis of variance (ANOVA) by Bonferroni's multiple comparison post-hoc test. All statistical analyses were performed with Prism 5 (GraphPad Software). *P*-value <0.05 was considered significant.

Conflict of Interest: The authors declare no competing financial interest.

Supporting Information Available: Rheological properties of the hybrid injectable GO/GelMA hydrogel, photo-cross-linkable nature of hydrogel and its biocompatibility, TEM images of GO nanocomplexes and zeta potential, cytotoxicity analysis with cells, GO/DNA release kinetics from hydrogel and the transfection efficiency, quantification of secretory VEGF protein overexpression, *in vivo* immunohistological and histological staining pictures. This material is available free of charge *via* the Internet at http://pubs.acs.org.

Acknowledgment. The authors acknowledge funding from the Presidential Early Career Award for Scientists and Engineers (PECASE), National Institutes of Health (HL092836, AR057837, DE021468, DE019024, EB012597, HL099073, EB008392) and MIT- Portugal Program (MPP-09Call-Langer-47). D.S.-T. acknowledges funding support from Collaborative Health Research Project, Canada and National Sciences & Engineering Research Council of Canada (NSERC) Strategic Project Grants from Canada. A.P. acknowledges postdoctoral award from FRQS (Fonds de recherche du Québec - Santé), Quebec, Canada. A.H. acknowledges the Postdoctoral award from Natural Sciences and Engineering Research Council of Canada.

REFERENCES AND NOTES

1. Slaughter, B. V.; Khurshid, S. S.; Fisher, O. Z.; Khademhosseini, A.; Peppas, N. A. Hydrogels in Regenerative Medicine. *Adv. Mater.* **2009**, *21*, 3307–3329.
2. Langer, R.; Vacanti, J. P. Tissue Engineering. *Science* **1993**, *260*, 920–926.
3. Khademhosseini, A.; Vacanti, J. P.; Langer, R. Progress in Tissue Engineering. *Sci. Am.* **2009**, *300*, 64–71.
4. Khademhosseini, A.; Langer, R.; Borenstein, J.; Vacanti, J. P. Microscale Technologies for Tissue Engineering and Biology. *Proc. Natl. Acad. Sci. U.S.A.* **2006**, *103*, 2480–2487.
5. Schukur, L.; Zorlutuna, P.; Cha, J. M.; Bae, H.; Khademhosseini, A. Directed Differentiation of Size-Controlled Embryoid Bodies towards Endothelial and Cardiac Lineages in RGD-Modified Poly(ethylene glycol) Hydrogels. *Adv. Healthcare Mater.* **2013**, *2*, 195–205.
6. Khetan, S.; Guvendiren, M.; Legant, W. R.; Cohen, D. M.; Chen, C. S.; Burdick, J. A. Degradation-Mediated Cellular Traction Directs Stem Cell Fate in Covalently Crosslinked Three-Dimensional Hydrogels. *Nat. Mater.* **2013**, *12*, 458–465.
7. Ashley, G. W.; Henise, J.; Reid, R.; Santi, D. V. Hydrogel Drug Delivery System with Predictable and Tunable Drug Release and Degradation Rates. *Proc. Natl. Acad. Sci. U.S.A.* **2013**, *110*, 2318–2323.
8. Jang, J. H.; Schaffer, D. V.; Shea, L. D. Engineering Biomaterial Systems to Enhance Viral Vector Gene Delivery. *Mol. Ther.* **2011**, *19*, 1407–1415.
9. Kong, H. J.; Liu, J.; Riddle, K.; Matsumoto, T.; Leach, K.; Mooney, D. J. Non-viral Gene Delivery Regulated by Stiffness of Cell Adhesion Substrates. *Nat. Mater.* **2005**, *4*, 460–464.
10. Cam, C.; Segura, T. Matrix-based Gene Delivery for Tissue Repair. *Curr. Opin. Biotechnol.* **2013**, *24*, 855–863.
11. Holladay, C.; Keeney, M.; Greiser, U.; Murphy, M.; O'Brien, T.; Pandit, A. A Matrix Reservoir for Improved Control of Non-viral Gene Delivery. *J. Controlled Release* **2009**, *136*, 220–225.
12. Schek, R. M.; Hollister, S. J.; Krebsbach, P. H. Delivery and Protection of Adenoviruses using Biocompatible Hydrogels for Localized Gene Therapy. *Mol. Ther.* **2004**, *9*, 130–138.
13. Paul, A.; Shao, W.; Abbasi, S.; Shum-Tim, D.; Prakash, S. PAMAM Dendrimer-Baculovirus Nanocomplex for Microencapsulated Adipose Stem Cell-Gene Therapy: *In Vitro* and *in Vivo* Functional Assessment. *Mol. Pharmaceutics* **2012**, *9*, 2479–2488.
14. Hu, W. W.; Wang, Z.; Hollister, S. J.; Krebsbach, P. H. Localized Viral Vector Delivery to Enhance *in Situ* Regenerative Gene Therapy. *Gene Ther.* **2007**, *14*, 891–901.
15. Paul, A.; Elias, C. B.; Shum-Tim, D.; Prakash, S. Bioactive Baculovirus Nanohybrids for Stent Based Rapid Vascular Re-endothelialization. *Sci. Rep.* **2013**, *3*, 2366.
16. Curtin, C. M.; Cunniffe, G. M.; Lyons, F. G.; Bessho, K.; Dickson, G. R.; Duffy, G. P.; O'Brien, F. J. Innovative Collagen Nano-hydroxyapatite Scaffolds Offer a Highly Efficient Non-viral Gene Delivery Platform for Stem Cell-Mediated Bone Formation. *Adv. Mater.* **2012**, *24*, 749–754.
17. Yin, L.; Song, Z.; Kim, K. H.; Zheng, N.; Gabrielson, N. P.; Cheng, J. Non-viral Gene Delivery *via* Membrane-penetrating, Mannose-Targeting Supramolecular Self-Assembled Nanocomplexes. *Adv. Mater.* **2013**, *25*, 3063–3070.
18. Kim, H.; Namgung, R.; Singha, K.; Oh, I. K.; Kim, W. J. Graphene oxide-Polyethylenimine Nanoconstruct as a Gene Delivery Vector and Bioimaging Tool. *Bioconjugate Chem.* **2011**, *22*, 2558–2567.
19. Feng, L.; Zhang, S.; Liu, Z. Graphene Based Gene Transfection. *Nanoscale* **2011**, *3*, 1252–1257.
20. Yin, D.; Li, Y.; Lin, H.; Guo, B.; Du, Y.; Li, X.; Jia, H.; Zhao, X.; Tang, J.; Zhang, L. Functional Graphene Oxide as a Plasmid-based Stat3 siRNA Carrier Inhibits Mouse Malignant

Melanoma Growth *in Vivo*. *Nanotechnology* **2013**, *24*, 105102.
21. Kim, H.; Kim, W. J. Photothermally Controlled Gene Delivery by Reduced Graphene Oxide-Polyethylenimine Nanocomposite. *Small* **2014**, *10*, 117–126.
22. Bitounis, D.; Ali-Boucetta, H.; Hong, B. H.; Min, D. H.; Kostarelos, K. Prospects and Challenges of Graphene in Biomedical Applications. *Adv. Mater.* **2013**, *25*, 2258–2268.
23. Feng, L.; Yang, X.; Shi, X.; Tan, X.; Peng, R.; Wang, J.; Liu, Z. Polyethylene Glycol and Polyethylenimine Dual-functionalized Nano-graphene Oxide for Photothermally Enhanced Gene Delivery. *Small* **2013**, *9*, 1989–1997.
24. Nichol, J. W.; Koshy, S. T.; Bae, H.; Hwang, C. M.; Yamanlar, S.; Khademhosseini, A. Cell-Laden Microengineered Gelatin Methacrylate Hydrogels. *Biomaterials* **2010**, *31*, 5536–5544.
25. Chen, Y. C.; Lin, R. Z.; Qi, H.; Yang, Y.; Bae, H.; Melero-Martin, J. M.; Khademhosseini, A. Functional Human Vascular Network Generated in Photocrosslinkable Gelatin Methacrylate Hydrogels. *Adv. Funct. Mater.* **2012**, *22*, 2027–2039.
26. Lin, R. Z.; Chen, Y. C.; Moreno-Luna, R.; Khademhosseini, A.; Melero-Martin, J. M. Transdermal Regulation of Vascular Network Bioengineering using a Photopolymerizable Methacrylated Gelatin Hydrogel. *Biomaterials* **2013**, *34*, 6785–6796.
27. Nikkhah, M.; Eshak, N.; Zorlutuna, P.; Annabi, N.; Castello, M.; Kim, K.; Dolatshahi-Pirouz, A.; Edalat, F.; Bae, H.; Yang, Y.; *et al.* Directed Endothelial Cell Morphogenesis in Micropatterned Gelatin Methacrylate Hydrogels. *Biomaterials* **2012**, *33*, 9009–9018.
28. Shin, S. R.; Bae, H.; Cha, J. M.; Mun, J. Y.; Chen, Y. C.; Tekin, H.; Shin, H.; Farshchi, S.; Dokmeci, M. R.; Tang, S.; *et al.* Carbon Nanotube Reinforced Hybrid Microgels as Scaffold Materials for Cell Encapsulation. *ACS Nano* **2012**, *6*, 362–372.
29. Shin, S. R.; Jung, S. M.; Zalabany, M.; Kim, K.; Zorlutuna, P.; Kim, S. B.; Nikkhah, M.; Khabiry, M.; Azize, M.; Kong, J.; *et al.* Carbon-Nanotube Embedded Hydrogel Sheets for Engineering Cardiac Constructs and Bioactuators. *ACS Nano* **2013**, *7*, 2369–2380.
30. Ramon-Azcon, J.; Ahadian, S.; Estili, M.; Liang, X.; Ostrovidov, S.; Kaji, H.; Shiku, H.; Ramalingam, M.; Nakajima, K.; Sakka, Y.; *et al.* Dielectrophoretically Aligned Carbon Nanotubes to Control Electrical and Mechanical Properties of Hydrogels to Fabricate Contractile Muscle Myofibers. *Adv. Mater.* **2013**, *25*, 4028–4034.
31. Shin, S. R.; Aghaei-Ghareh-Bolagh, B.; Dang, T. T.; Topkaya, S. N.; Gao, X.; Yang, S. Y.; Jung, S. M.; Oh, J. H.; Dokmeci, M. R.; Tang, X. S.; *et al.* Cell-Laden Microengineered and Mechanically Tunable Hybrid Hydrogels of Gelatin and Graphene Oxide. *Adv. Mater.* **2013**, *25*, 6385–6391.
32. Cha, C.; Shin, S. R.; Gao, X.; Annabi, N.; Dokmeci, M. R.; Tang, X. S.; Khademhosseini, A. Controlling Mechanical Properties of Cell-Laden Hydrogels by Covalent Incorporation of Graphene Oxide. *Small* **2014**, *10*, 514–523.
33. Mihaila, S. M.; Gaharwar, A. K.; Reis, R. L.; Marques, A. P.; Gomes, M. E.; Khademhosseini, A. Photocrosslinkable Kappa-carrageenan Hydrogels for Tissue Engineering Applications. *Adv. Healthcare Mater.* **2013**, *2*, 895–907.
34. Seif-Naraghi, S. B.; Singelyn, J. M.; Salvatore, M. A.; Osborn, K. G.; Wang, J. J.; Sampat, U.; Kwan, O. L.; Strachan, G. M.; Wong, J.; Schup-Magoffin, P. J. Safety and Efficacy of an Injectable Extracellular Matrix Hydrogel for Treating Myocardial Infarction. *Sci. Transl. Med.* **2013**, *5*, 173ra25.
35. Liu, Z.; Wang, H.; Wang, Y.; Lin, Q.; Yao, A.; Cao, F.; Li, D.; Zhou, J.; Duan, C.; Du, Z.; *et al.* The Influence of Chitosan Hydrogel on Stem Cell Engraftment, Survival and Homing in the Ischemic Myocardial Microenvironment. *Biomaterials* **2012**, *33*, 3093–3106.
36. Shuman, J. A.; Zurcher, J. R.; Sapp, A. A.; Burdick, J. A.; Gorman, R. C.; Gorman, J. H., 3rd; Goldsmith, E. C.; Spinale, F. G. Localized Targeting of Biomaterials Following Myocardial Infarction: A Foundation to Build on. *Trends Cardiovasc. Med.* **2013**, *23*, 301–311.
37. MacArthur, J. W., Jr.; Purcell, B. P.; Shudo, Y.; Cohen, J. E.; Fairman, A.; Trubelja, A.; Patel, J.; Hsiao, P.; Yang, E.; Lloyd, K.; *et al.* Sustained Release of Engineered Stromal Cell-derived Factor 1-alpha from Injectable Hydrogels Effectively Recruits Endothelial Progenitor Cells and Preserves Ventricular Function After Myocardial Infarction. *Circulation* **2013**, *128*, S79–S86.
38. Johnson, T. D.; Christman, K. L. Injectable Hydrogel Therapies and Their Delivery Strategies for Treating Myocardial Infarction. *Expert Opin. Drug Delivery* **2013**, *10*, 59–72.
39. Tous, E.; Purcell, B.; Ifkovits, J. L.; Burdick, J. A. Injectable Acellular Hydrogels for Cardiac Repair. *J. Cardiovasc. Transl. Res.* **2011**, *4*, 528–542.
40. Ifkovits, J. L.; Tous, E.; Minakawa, M.; Morita, M.; Robb, J. D.; Koomalsingh, K. J.; Gorman, J. H., 3rd; Gorman, R. C.; Burdick, J. A. Injectable Hydrogel Properties Influence Infarct Expansion and Extent of Postinfarction Left Ventricular Remodeling in an Ovine Model. *Proc. Natl. Acad. Sci. U.S.A.* **2010**, *107*, 11507–11512.
41. Paul, A.; Shao, W.; Shum-Tim, D.; Prakash, S. The Attenuation of Restenosis Following Arterial Gene Transfer Using Carbon Nanotube Coated Stent Incorporating TAT/DNA-(Ang1+Vegf) Nanoparticles. *Biomaterials* **2012**, *33*, 7655–7664.
42. Paul, A.; Binsalamah, Z. M.; Khan, A. A.; Abbasia, S.; Elias, C. B.; Shum-Tim, D.; Prakash, S. A Nanobiohybrid Complex of Recombinant Baculovirus and Tat/DNA Nanoparticles for Delivery of Ang-1 Transgene in Myocardial Infarction Therapy. *Biomaterials* **2011**, *32*, 8304–8318.
43. Gerczuk, P. Z.; Kloner, R. A. An Update on Cardioprotection: A Review of the Latest Adjunctive Therapies To Limit Myocardial Infarction Size in Clinical Trials. *J. Am. Coll. Cardiol.* **2012**, *59*, 969–978.
44. Windecker, S.; Bax, J. J.; Myat, A.; Stone, G. W.; Marber, M. S. Future Treatment Strategies in ST-segment Elevation Myocardial Infarction. *Lancet* **2013**, *382*, 644–657.
45. Nabel, E. G.; Braunwald, E. A Tale of Coronary Artery Disease and Myocardial Infarction. *N. Engl. J. Med.* **2012**, *366*, 54–63.
46. Takahashi, K.; Ito, Y.; Morikawa, M.; Kobune, M.; Huang, J.; Tsukamoto, M.; Sasaki, K.; Nakamura, K.; Dehari, H.; Ikeda, K.; *et al.* Adenoviral-delivered Angiopoietin-1 Reduces the Infarction and Attenuates the Progression of Cardiac Dysfunction in the Rat Model of Acute Myocardial Infarction. *Mol. Ther.* **2003**, *8*, 584–592.
47. Tao, Z.; Chen, B.; Tan, X.; Zhao, Y.; Wang, L.; Zhu, T.; Cao, K.; Yang, Z.; Kan, Y. W.; Su, H. Coexpression of VEGF and Angiopoietin-1 Promotes Angiogenesis and Cardiomyocyte Proliferation Reduces Apoptosis in Porcine Myocardial Infarction (MI) Heart. *Proc. Natl. Acad. Sci. U.S.A.* **2011**, *108*, 2064–2069.
48. Moore, C. S.; Rao, V. T.; Durafourt, B. A.; Bedell, B. J.; Ludwin, S. K.; Bar-Or, A.; Antel, J. P. miR-155 as a Multiple Sclerosis-Relevant Regulator of Myeloid Cell Polarization. *Ann. Neurol.* **2013**, *74*, 709–720.
49. O'Connell, R. M.; Rao, D. S.; Baltimore, D. microRNA Regulation of Inflammatory Responses. *Annu. Rev. Immunol.* **2012**, *30*, 295–312.
50. Dai, R.; Ahmed, S. A. MicroRNA, a New Paradigm for Understanding Immunoregulation, Inflammation, and Autoimmune Diseases. *Transl. Res.* **2011**, *157*, 163–179.
51. Nazari-Jahantigh, M.; Wei, Y.; Schober, A. The role of microRNAs in arterial remodelling. *Thromb. Haemost.* **2012**, *107*, 611–618.
52. Boon, R. A.; Iekushi, K.; Lechner, S.; Seeger, T.; Fischer, A.; Heydt, S.; Kaluza, D.; Treguer, K.; Carmona, G.; Bonauer, A.; *et al.* MicroRNA-34a Regulates Cardiac Ageing and Function. *Nature* **2013**, *495*, 107–110.
53. Li, R.; Yan, G.; Li, Q.; Sun, H.; Hu, Y.; Sun, J.; Xu, B. MicroRNA-145 Protects Cardiomyocytes against Hydrogen Peroxide (H_2O_2)-induced Apoptosis Through Targeting the Mitochondria Apoptotic Pathway. *PLoS One* **2012**, *7*, e44907.
54. Chowdhury, S. M.; Kanakia, S.; Toussaint, J. D.; Frame, M. D.; Dewar, A. M.; Shroyer, K. R.; Moore, W.; Sitharaman, B. *In vitro* Hematological and *in Vivo* Vasoactivity Assessment of Dextran Functionalized Graphene. *Sci. Rep* **2013**, *3*, 2584.

55. Yang, K.; Gong, H.; Shi, X.; Wan, J.; Zhang, Y.; Liu, Z. *In vivo* Biodistribution and Toxicology of Functionalized Nano-Graphene Oxide in Mice After Oral and Intraperitoneal Administration. *Biomaterials* **2013**, *34*, 2787–2795.
56. Yang, K.; Wan, J.; Zhang, S.; Zhang, Y.; Lee, S. T.; Liu, Z. *In Vivo* Pharmacokinetics, Long-Term Biodistribution, and Toxicology of PEGylated Graphene in Mice. *ACS Nano* **2011**, *5*, 516–522.
57. Liu, Y.; Luo, Y.; Wu, J.; Wang, Y.; Yang, X.; Yang, R.; Wang, B.; Yang, J.; Zhang, N. Graphene Oxide Can Induce *in Vitro* and *in Vivo* Mutagenesis. *Sci. Rep.* **2013**, *3*, 3469.
58. Qu, G.; Liu, S.; Zhang, S.; Wang, L.; Wang, X.; Sun, B.; Yin, N.; Gao, X.; Xia, T.; Chen, J. J.; Jiang, G. B. Graphene Oxide Induces Toll-like Receptor 4 (TLR4)-Dependent Necrosis in Macrophages. *ACS Nano* **2013**, *7*, 5732–5745.
59. Paul, A.; Srivastava, S.; Chen, G.; Shum-Tim, D.; Prakash, S. Functional Assessment of Adipose Stem Cells for Xeno-transplantation using Myocardial Infarction Immunocompetent Models: Comparison with Bone Marrow Stem Cells. *Cell Biochem. Biophys.* **2013**, *67*, 263–273.